Published in final edited form as:
Environ Sci Technol. 2010 November 1; 44(21): 8236–8242. doi:10.1021/es101601s.

Debromination of Polybrominated Diphenyl Ethers by Nanoscale Zerovalent Iron: Pathways, Kinetics, and Reactivity

Yuan Zhuang, **Sungwoo Ahn**, and **Richard G. Luthy***
Department of Civil and Environmental Engineering, Stanford University, Stanford, CA 94305-4020

Abstract

The debromination of selected polybrominated diphenyl ethers (PBDEs) by nanoscale zerovalent iron particles (nZVI) was studied to investigate the degradation pathways and the reaction kinetics of the PBDEs. The primary PBDE investigated was 2,3,4-tribromo diphenyl ether (BDE 21) to assess degradation pathways. nZVI could effectively debrominate the selected PBDEs into lower brominated compounds and diphenyl ether, a completely debrominated form of PBDEs. The susceptibility of the meta-bromine by nZVI was observed from the debromination tests for PBDEs with single-flanked (2,3-diBDE and 3,4-diBDE) and unflanked (three monoBDEs) bromines. The stepwise debromination from n-bromo- to (n-1)-bromodiphenyl ether was observed as the dominant reaction process, although simultaneous multistep debromination seemed to be plausible for di-BDEs having two bromines adjacent on the same phenyl ring. The reaction rate constants were estimated by assuming the reaction between PBDEs and nZVI was a pseudo-first order reaction and the rates decreased with fewer bromine substituents. The reaction rate constants were correlated with the heat of formation and the energy of the lowest unoccupied molecular orbital of the corresponding compounds, and these appear to be useful descriptors of relative reaction rates among PBDE homologue groups.

Introduction

Polybrominataed diphenyl ethers (PBDEs) are a class of brominated flame-retardants (BFRs) extensively used over past several decades in various industrial and consumer products. Unlike other reactive BFRs that are chemically bound to polymers, PBDEs are simply blended with the polymer during its formation and thus may more readily migrate from products to the environment (1). The levels of the PBDEs in the environment have increased exponentially in the past 30 years (2). Among the pool of environmentally-important PBDE congeners, the less brominated congeners are more widespread as they have been observed in areas distant from their known use of production, e.g., the Arctic (3), and more bioaccumulative probably due to their smaller molecular sizes or smaller depuration rates (4,5), and more toxic (6), compared to higher brominated congeners.

For these reasons it is important to develop effective and feasible remediation technologies for PBDE contamination. Nanoscale zerovalent iron (nZVI) is a strong reducing agent for many organic contaminants. Due to the larger specific surface area, nZVI (20–100 nm in diameter) can greatly improve reaction rates compared to micro-scale ZVI (1–50 μm in diameter). Recent studies show that nZVI can degrade an array of environmental contaminants (7), however, chlorinated or brominated alicyclic and aromatic compounds such as PCBs and PBDEs, which

*Corresponding author phone: (650) 721-2165; fax: (650) 725-9720; luthy@stanford.edu.

Supporting Information Available
This information is available free of charge via the Internet at http://pubs.acs.org/.

react slowly with nZVI and often generate more intermediates and byproducts, have received far less attention. Currently, only limited information is available for PBDE debromination by nZVI, mainly for the fully brominated diphenyl ether, deca-BDE (BDE 209) (8,9). Keum and Li tested six PBDEs using micro-ZVI (10). nZVI was tested to debrominate BDE 209 and determine the reaction products with respect to bromine substitution positions, but the presence of unidentified peaks made it difficult to conclusively confirm the positional preference or pathways for the debromination of the compound (8,9).

In this study, we selected 2,3,4-tribromodiphenyl ether (BDE 21) that has one bromine at each of the ortho-, meta-, and para-positions on one side of the diphenyl ether to investigate the reaction of PDBEs with nZVI. A series of contact experiments was conducted using BDE 21 and its debromination product congeners to study reaction kinetics and position preference of debromination among different mono-, di-BDE homologues and BDE 21. Also, correlation analyses between the estimated reaction rate constants and molecular properties were made to assess reaction mechanisms among the full range of PBDEs.

Experimental Section

Nanoscale ZVI Synthesis and Characterization

nZVI particles were synthesized by aqueous phase reduction of dissolved ferrous sulfate by an excess of sodium borohydride with a slight modification from the method previously reported by Liu et al. (11), and dried by freeze-dryer. A detailed description of the synthesis method is included in the Supporting Information.

The morphology of the iron particles was investigated using transmission electron microscopy (TEM, Tecnai G2 F20 X-TWIN, FEI Company, Hillsboro, OR) with energy dispersive x-ray detector (EDS). Particles were dispersed in methanol by sonication and dripped onto a lacey carbon film for the analysis. X-ray diffraction (XRD) analysis with Fe K edge (7111 eV) radiation was performed on a powder diffractometer at the Stanford Synchrotron Radiation Lightsource (Stanford, CA). X-ray photoelectron spectroscopy (XPS, PHI VersaProbe Scanning XPS, Physical Electronics, Inc., Chanhassen, MN) analysis with Al(K) radiation (1486 eV) was performed to survey iron speciation. The N_2-BET specific surface areas of the synthesized particles were measured using a Coulter SA 3100 surface area and pore size analyzer (Coulter Corporation, Miami, FL). The fraction of zerovalent iron (Fe^0) within the particles was determined by quantifying hydrogen gas evolved, using a Trace Analytical RGA3 reduction gas analyzer (Trace Analytical, Pittsburgh, PA) after digesting an aliquot of the particles with 10 ml of concentrated HCl (36.5 – 38.0%, EMD) solution in a serum bottle overnight. The Fe^0 content was calculated assuming that 1 mole of H_2 is produced per mole of Fe^0 from the acid digestion as represented in Eq. 1.

$$Fe^0 + 2H^+ \rightarrow Fe^{2+} + H_2 \uparrow \quad \text{(Eq. 1)}$$

The total iron and boron contents of the particle were determined from inductively coupled plasma-atomic emission spectrometry (ICP-AES, IRIS Advantage/1000, TJA Solutions, Franklin, MA) by following EPA Method 6010B.

Debromination Experiments

Table 1 lists the shorthand nomenclature for the PBDEs investigated. 1 g of nZVI was added to a serum vial containing 10 ml of the individual PBDE (Accustandard) stock solution at the known concentration. The PBDE solutions were prepared in an acetone/milli-Q water solution (50:50, v/v) with 0.4% sodium azide added to minimize microbial degradation. The sample

bottle was sealed with a Teflon/silica septa, and sonicated in a water bath for 5 minutes to disperse the particles. The prepared samples were placed on a horizontal shaker at 60 rpm and covered to avoid photodegradation. At preselected time intervals, samples were sacrificed to measure the concentrations of the parent compound and the reaction products. The samples were extracted three times using toluene and the collected extract was dried using anhydrous Na_2SO_4 (granular, 10–60 mesh, Fisher), and further concentrated down to 1 ml under a gentle N_2 stream. PCB 15 (Ultra scientific), an internal standard, was spiked into each sample prior to analyses for quantification purposes. All samples were prepared in triplicate.

Instrumental Analysis

PBDEs in the extracts were analyzed using gas chromatography with mass spectrometric detector (GC-MSD, Agilent 6890N-5973N, Palo Alto, CA) equipped with a HP-5ms capillary column (30.0 m × 250 μm × 0.25 μm). 1 μL of the sample was injected in splitless mode with the inlet maintained at 250 °C. The oven was held initially at 60 °C for 2 min, increased at the rate of 4 °C/min to the final temperature of 250 °C, which was held for 20 min. Helium was used as carrier gas at 1 ml/min. The interface temperature for MSD and ion source temperature were both set at 280 °C. The mass spectrometer was in the selective ion monitoring (SIM) mode at the electron impact energy of 69.9 eV

Results and Discussions

Particle Characterization

Figure S1 (in Supporting Information) shows the TEM images of the synthesized nZVI particles. Because of magnetic effects between the nanoparticles, the particles exist as aggregates of spherical particles in the size range of 20 – 100 nm. The average crystallized iron grain size estimated from XRD patterns was approximately 2 nm, showing a short-range ordered structure of iron particles (12). Atomic lengths determined from electron diffraction patterns from TEM and peaks identified on the XRD patterns (Figure S2) confirmed that the aggregates are composed mainly of zero-valent iron. The Fe 2p3 spectra of nZVI from XPS (Figure S3) show a strong signal of oxidized iron on the surface besides zero-valent iron, indicating a core-shell morphology where the surface of nZVI is covered by a layer of iron oxide film, mainly Fe_2O_3. Since the nanoparticle is highly reactive, the surface oxidation is likely to happen during any step of the synthesis and storing the particles afterwards. The estimated shell thickness of iron oxide film in the aggregates was approximately 3 nm as calculated from Eq. S1. The TEM image also confirmed the calculated thickness (Figure S1 (b)).

ICP-AES analysis revealed that the synthesized nZVI comprises approximately 76% iron in any form and 5% boron by weight, with the remaining 19% considered mostly to be oxygen in iron oxides and other impurities. Similar compositions have been reported in other studies (13,14). Among total iron, 72% is zerovalent iron, corresponding to approximately 55% of total mass in the entire nanoparticles. The remaining iron exists in oxide forms. The oxide layer covering zerovalent iron may sacrifice reactivity to a certain degree compared to fresh iron, but it may protect the zerovalent iron core from further oxidation as well.

The synthesized nZVI particles had a BET surface area of 15.5 ± 0.5 m^2/g and were essentially nonporous, which agrees with data reported in the literature (13,15,16). Somewhat larger BET surface areas (30 – 37 m^2/g) and smaller particle sizes (20 – 40 nm) are reported in studies that employed similar synthesis methods (14,17). The synthesis conditions, such as solvents, pH, and drying, are believed to affect the size as well as surface area of the resulting nanoparticles (18,19). Assuming nZVI to be spherical, calculation (Eq. S2) shows that the nZVI particles

would have a specific surface area of about 13 m^2/g with an average diameter of 60 nm. Thus, the calculated and measured surface areas show reasonable agreement.

Debromination Pathways

nZVI could rapidly debrominate BDE 21. BDE 21 completely disappeared in the system within 4 days, resulting in its lower brominated intermediates (di- and mono-BDEs) and diphenyl ether (DE), the completely debrominated form of PBDEs. Figure 1 shows the changes in the composition of the compounds in the system during experimental observation, up to 1 month. Di-BDEs were the dominant forms of BDEs in the early stages of the reaction and they continued to increase up to 4 days. After the BDE 21 concentration dropped to a low level in the system, the di-BDEs started to decrease and the trend continued throughout the period of experimental observation. The production of mono-BDEs and DE were minimal during the period that the increase of di-BDEs was observed, and mono-BDEs and DE started to accumulate with the transformation of di-BDEs. BDE 5 (2,3-dibromodiphenyl ether) and BDE 12 (3,4-dibromodiphenyl ether) are shown as their sum because they cannot be separately identified by GC-MSD due to their similar molecular properties.

The debromination pathways were further investigated by conducting individual debromination tests on the relevant intermediate di-BDEs and mono-BDEs (shown in Figure S4). As a group, the debromination tests with individual mono-BDEs by nZVI showed the slowest reaction among the tested BDEs with less than 10% of mono-BDEs degraded within 40 days with minimal amount of DE detected (shown in Figure S4(a) and (b)). Compared to mono-BDEs, a considerable amount of DE was formed simultaneously along with mono-BDEs from the debromination of BDE 5 and 12 (shown in Figure S4(c) and (d)), whereas far less DE was produced compared to mono-BDEs from BDE 7 (2,4-dibromodiphenyl ether) (shown in Figure S4(e)). The debromination trend, in general, may indicate that the debromination of PBDEs by nZVI is a stepwise reaction, from n-BDE to (n-1)-BDE. Keum and Li previously reported that stepwise dehalogenation was dominant when BDE 209 was contacted with powdery micro-ZVI (10). Also, similar stepwise dechlorination of PCBs by micro-ZVI in water has been observed at high temperature and pressure (20). However, the debromination of BDE 5 and 12 seems to suggest that near simultaneous loss of ortho- and meta-, or meta- and para-bromines might be possible. If stepwise debromination was a dominant pathway for BDE 5 and 12, the increase in DE concentration should have been seen after the increase of mono-BDEs. BDE 5 and 12 have two bromines adjacent to each other and their molecular structures may increase a chance for both bromines to simultaneously anchor to the surface of nZVIs, leading to a rapid sequential two-step or simultaneous debromination. Concerted transformations were also reported for di- and tri-chlorobenzenes (21) and di-chlorobiphneyls (22) when the compounds were reduced by a catalyzed ZVI (ZVI/Pd). But none was reported for brominated aromatic compounds by ZVI before.

For the PBDEs we studied, we observed that the bromine at the meta-position was the most susceptible to the debromination by nZVI. The test on BDE 21 showed that, among the intermediates, BDE 7 that lost the meta-bromine showed higher concentration than the other two di-BDEs (BDE 5 and 12). Although the susceptibility of meta-bromine might be caused by double-flanking for BDE 21, this viewpoint on relative reactivity was determined in general by BDEs with single-flanked (BDE 5 and 12) and unflanked (BDE 1, 2, 3) bromines. When there was a meta-bromine present in di-BDEs (BDE 5 and 12), it was clear that the meta-bromine undergoes the debromination preferentially, resulting in less BDE 2 (3-monobromodiphenyl ether) production compared to the other mono-BDEs. Observations from the debromination tests on mono-BDEs, BDE 2 showed faster degradation among mono-BDEs although the differences were very small. The susceptibility of the meta-position towards reaction could be viewed as favoring nucleophilic substitution; the combined effects of the

ether bond and the bromines on the electron density of a phenyl ring may make the meta-bromine more vulnerable to electron attack compared to ortho- or para-bromines within the same ring. The tenaciousness of para-bromines for reduction by ZVI was reported in the tests with BDEs 28, 47, 66, 100 (10), and the test with BDE 209 based on confidently identified hepta- to di-BDE products (8,9). But the susceptibility of meta-bromines was not clearly concluded as all the PBDEs in those tests tested have bromines on both sides of the phenyl rings, and only BDE 66 and 209 have meta-bromines. Nevertheless, the preferential debromination of meta-bromines was revealed in accumulation of products (2,3′,4,4′,6-BDE119, 2,2′,4,4′,5,6′-BDE154, 2,2′3,4,4′,5′,6-BDE183, 2,2′,3,4,4′,6,6′-BDE184, 2,4,4′,6-BDE75, 2,2′,4,4′-BDE47, 2,2′,4-BDE17, 2,4,4′-BDE28) from BDE 209 that are mainly ortho-brominated (9). In our study, the preferential difference between ortho- and para-bromines seems to be slight. The debromination test on BDE 7 shows the tenaciousness of ortho-bromines by nZVI, resulting in abundance of BDE 1 (2-monobromodiphenyl ether) compared to BDE 3 (4-monobromodiphenyl ether). Based on byproducts formation from the debromination of BDE 21, and di- and mono-BDEs by nZVI, the positional preference exhibits the following trend: meta $\gg$ para $\geq$ ortho. This position preference might not be true for other congeners, especially if steric effects caused by adjacent bromines, oxygen and the phenyl ring play an important role here. The observation in this study is apparently in contrast to the positional preference reported for PCB dechlorination by nZVI, where para-chlorine removal was predominant for tri- and tetra-chlorobiphenyls (14). This may indicate that the oxygen atom between the two rings affects the relative vulnerability of bromines at different positions as it renders PBDE molecules more nonlinear and nonplanar (23).

Mass balances were calculated to consider any possibility of irreversible sorption or non-extractable compound formation. The recoveries were quantitative, ranging from 90 – 98%, throughout most of the tests except that tests on BDE 5 and 12 showed lower recovery (70–75%), and BDE 21 (around 65%). The mass balance for the BDE 21 tests became constant after 4 days once BDE 21 disappeared. There might be a similar mechanisms contributing to the coincidence of mass loss for BDE 5, 7 and 21, all of which have adjacent bromines. The possibility of forming other degradation compounds by other transformation mechanisms cannot be ruled out. Possible reactions were indicated in the following studies: hydroxylation or the cleavage of the ether bond of PBDEs in biotransformation process (24,25); the intramolecular cyclization by the dissociation of C-Br bond and the cleavage of ether bond of DE in photodegradation processes (26,27); oxidation process with ZVI in oxygen-rich conditions in study of pesticides (28); and formation of polychlorinated dibenzofurans (PCDFs) in PCB pyrolysis (29). Efforts were made to prove the existence of unknown intermediates with available analytical methods, but none of those products was identified.

Based on our observations, the main debromination pathways of BDE 21 by nZVI are proposed in Figure 2, for which the dominant degradation pathways are represented with thicker arrows. The degradation byproducts from BDE 5 show an unexpected outcome; instead of BDE 1 and BDE 2, BDE 2 and BDE 3 were detected as byproducts and no BDE 1 was detected. Considering the complexity of heterogeneous surface reactions, one possible explanation for this outcome could be a sigmatropic [1,5] shift of bromine, which is not represented by simple and discrete electron transfers involving intramolecular migration of the substituent with simultaneous rearrangement of the π system. Minkin et al. showed bromine migration over the cyclopentadiene ring due to sigmatropic shift in reaction of 5-methyl-1,2,3,4-tetramethoxycarbonylcyclopendadien with N-bromosuccinimide (30). Similarly, a rearrangement reaction known as [1,2]-hydrogen shift was reported during the pyrolysis of PCB isomers to PCDFs (29) and metabolic hydroxylation of PCBs (31,32). Another possibility is that an activated form of DE is formed from the simultaneous debromination of PBDEs, which re-acquires available bromine at its para-position wherein the intermolecular repulsion is minimal. Further investigation is needed to answer this physical organic chemistry question.

Nevertheless, this is the first research discovering bromine shift by ZVI under ambient conditions. The mechanisms underlying this bromine shift, which favors the formation of para-brominated DEs, might further contribute to the persistence of para-bromines in PBDEs.

Debromination Kinetics

The debromination tests on BDE 21, 12, 7, 5, 3, 2, and 1 by nZVI are described well by the pseudo-first-order kinetic model as represented in Eq. S3. The observed rate constants decrease with the number of bromines, which is in accord with findings from PBDE debromination by micro-ZVI (10). Similar tendencies have been observed for PCBs, dioxins, and aliphatic halides (33–35). The bromines act as electron-withdrawing groups that reduce the electron density on the benzene ring. An increasing number of bromines would lower the electron density on the ring and make the molecule more susceptible to nucleophilic substitution.

It is widely accepted that the higher reactivity of nZVI mainly comes from its larger specific surface area compared to micro-ZVI. Thus, normalizing reaction rates with respect to specific surface area is commonly used to compare reaction rates with different-sized ZVI materials for heterogeneous reactions (12,14). However, choosing specific surface area (SSA) to normalize the reaction rates should be used with caution, especially in the case of experimentally measured surface area such as BET-SA. Some researchers reported that the physical characteristics of the particles by itself, such as SSA, could not explain reactivity differences between the different forms of Fe^0 they tested (36,37). The use of nZVI content (mass concentration) normalized reaction rate might be considered as an alternative when surface area differences among particles under comparison are not drastic. Liu et al. reported that tests using a commercially available nZVI showed a good correlation between different initial Fe^0 contents and observed rate constants (38). Nevertheless, considering the wide range of size differences in ZVIs, SSA normalized rate constants remain an effective way to account for the surface area effect. For example, Li et al. attributed their enhanced debromination reaction rate of BDE 209 by the resin-bound nZVI to the larger surface areas of the nanoparticles over micro-ZVI (8). In order to compare reaction rates among different studies, nZVI mass concentration normalized and SSA normalized rate constants were calculated in this study using Eq. S4.

The rate constants (observed, nZVI mass concentration normalized, and SSA normalized) for PBDEs are summarized in Table 1 using data from this study as well as data from Li et al. and Keum and Li (8,10). Generally, the rates increase by one order of magnitude with one more degree of bromine substitution. There were, however, no common PBDEs among all three studies. The only comparable compounds were BDE 7 (this study and micro-ZVI) and BDE 209 (resin-bound nZVI and micro-ZVI). When k_m values of BDE 7 and BDE 209 were compared with k_{SA} values, it seems to suggest that the higher surface area of nZVI plays a more important role than its mass. Two to three orders of magnitude difference in the rate constants, k_m, between nZVI and micro-ZVI were reduced to a factor of four to seven when the rates were normalized using SSA. All the rates in this study were calculated utilizing data collected up to 40 days. In contrast, Li et al. and Keum et al. used data collected from a few hours, and 3 days, respectively. The data collected in shorter period reaction tests might contribute to greater SSA normalized rate constants considering the deactivation and aging of nZVI over the course of the reaction. This would partially explain why the SSA normalized debromination rate for BDE 7 in this study is about four times slower than micro-ZVI, and BDE 209 in resin-bound nZVI is around seven times faster than micro-ZVI. In addition, the environmental conditions, such as solution, pH, temperature, which were not all the same among these three studies, would further contribute to such differences.

Based on the proposed debromination pathways of BDE 21 by nZVI as shown in Figure 2, eight differential equations are deduced to regress the change of BDE 21 and its debrominated

products. The entire set of the equations and its solution can be found in the Supporting Information (Eq. S5). The reaction rates of all compounds involved in the debromination reactions were solved by minimizing the sum of square difference between model-predicted and experimental values using MATLAB. Multiple solutions for the eleven unknown rate constants were possible out of the eight equations. Sensitivity tests on the debromination rates showed that the reaction rates of mono-BDEs were the least sensitive to estimation of the other reaction rates due to their small values. Thus, it seems reasonable to choose the three rate constants for mono-BDEs as predetermined from the individual mono-BDE experiments. The lines in Figure 1 represent the modeling results and they fit the data well, which indicates the equations deduced from the proposed degradation pathways describe the system properly. It should be noted that, for di-BDEs, the rate constants from the BDE 21 test were three to four times larger than those from the individual di-BDEs debromination tests (Table S1). Considering that the main dehalogenation reaction is stepwise and sequential, the intermediate di-BDEs could be unstable, possibly in the activated state and may result in the faster reactions for the intermediates. For comparison, an alternative model S1 in Supporting Information was built up by considering all possible debromination pathways for BDE 21 and assuming the debromination kinetics for intermediates were the same as those in individual debromination tests as parent. But the fittings weren't as well as those represented in Figure 1 derived from simplified pathways shown in Figure 2.

Property-reactivity relationship

Molecular properties of organic compounds can provide valuable insight into the reaction mechanisms and help understand the fate of the compounds in the environment. The dependence of the reductive dehalogenation potential on certain molecular properties has been studied for halogenated compounds (10,33,35). Using molecular properties, such as the Gibbs free energy of formation, lowest unoccupied molecular orbital energies (E_{LUMO}), electron affinities, and electron reduction potentials, as the descriptor variables to correlate with rates of reactions are extremely useful for compounds such as PBDEs and PCBs, which have numerous congeners. There are a few studies on theoretical calculations of chemical properties of PBDEs (23,39,40), however, the correlation between the compounds' molecular properties and the reaction of the compounds with nZVI or micro-ZVI is limited due to the lack of available experimental data. Hence, the available data on the reactions between ZVI and PBDEs including the results from this study are collected and compared. Kinetic data obtained from other publications were reprocessed for comparison purposes (Table 1) and the values of H_f and E_{LUMO} for corresponding PBDEs were obtained from Hu et al. (39). Additional data for BDE 21 and BDE 5 were obtained from direct communication with J. Hu. A good correlation was found between the nZVI mass normalized debromination rates and H_f (R^2= 0.889 for nZVI, R^2=0.786 for ZVI) or E_{LUMO} (R^2= 0.940 for nZVI, R^2= 0.759 for ZVI) with the data collected (Figure S5). Two to three orders of magnitude difference in k_m values between the nZVI data (represented in solid lines) and the micro-ZVI data (represented in dotted lines) mainly reflects the differencesin the specific surface area. SSA normalized rates, k_{SA}, also show a good correlation with respect to H_f (R^2=0.805) or E_{LUMO} (R^2=0.920) (Figure 4). Therefore, when the particle size difference is substantial, k_{SA} may provide a more appropriate basis for comparison.

H_f is a thermodynamic property that can represent the chemical stability of a compound and it can also be regarded as a driving force of the reaction. As seen in Figure 3(a), H_f values of PBDE congeners increase with an increasing number of bromines and this indicates thermodynamic instability of highly brominated compounds. The lower brominated compounds, in contrast, show chemical stability against reductive debromination. E_{LUMO}, is a widely used quantum chemical descriptor that plays a major role in governing many chemical reactions, and this has been used to explain the reduction of chlorinated aliphatic compounds

(35). The LUMO is the frontier molecular orbital where electron transfer takes place. Thus, the energy of this orbital is directly related to the electron affinity and used as an indicator of the susceptibility of the molecule towards nucleophilic attack, a driving force for reaction (41). The highly brominated PBDEs show lower E_{LUMO} values as shown in Figure 3(b), indicating that the highly brominated diphenyl ethers are more reactive towards an electron donor, nZVI in this study. A good correlation between the reaction rates and E_{LUMO} suggests direct electron transfer as a major reaction mechanism between PBDEs and nZVI. Although the differences in H_f, E_{LUMO}, and reaction rates are apparent between homologues, the congeners within each homologue show relatively small differences. Other molecular properties such as intermolecular repulsion and steric hindrance effects might be considered to further elucidate the details of their debromination mechanisms.

Supplementary Material

Refer to Web version on PubMed Central for supplementary material.

Acknowledgments

The authors thank professor Jiwei Hu from Guizhou Normal University, China, for sharing useful information on the molecular properties of PBDEs. The authors also thank Angelia Seyfferth (Stanford University) for performing XRD analysis of the samples. This work was supported by Superfund Research Program, National Institute of Health (R01ES1614).

Literature Cited

1. Alaee M, Arias P, Sjodin A, Bergman A. An overview of commercially used brominated flame retardants, their applications, their use patterns in different countries/regions and possible modes of release. Environ Int 2003;29(6):683–689. [PubMed: 12850087]
2. Hites RA. Polybrominated diphenyl ethers in the environment and in people: A meta-analysis of concentrations. Environ Sci Technol 2004;38(4):945–956. [PubMed: 14998004]
3. Hale RC, Alaee M, Manchester-Neesvig JB, Stapleton HM, Ikonomou MG. Polybrominated diphenyl ether flame retardants in the North American environment. Environ Int 2003;29(6):771–779. [PubMed: 12850095]
4. Sellstrom U, De Wit CA, Lundgren N, Tysklind M. Effect of sewage-sludge application on concentrations of higher-brominated diphenyl ethers in soils and earthworms. Environ Sci Technol 2005;39(23):9064–9070. [PubMed: 16382926]
5. Ciparis S, Hale RC. Bioavailability of polybrominated diphenyl ether flame retardants in biosolids and spiked sediment to the aquatic oligochaete, Lumbriculus variegatus. Environ Toxicol Chem 2005;24 (4):916–925. [PubMed: 15839567]
6. U.S. Department of Health and Human Services, Public Health Service Agency for Toxic Substances and Disease Registry. Toxicological Profile for Polybrominated Biphenyls and Polybrominated Diphenyl Ethers (PBBs and PBDEs). ATSDR; Atlanta, GA: 2004.
7. Li XQ, Elliott DW, Zhang WX. Zero-valent iron nanoparticles for abatement of environmental pollutants: Materials and engineering aspects. Crit Rev Solid State 2006;31(4):111–122.
8. Li A, Tai C, Zhao ZS, Wang YW, Zhang QH, Jiang GB, Hu JT. Debromination of decabrominated diphenyl ether by resin-bound iron nanoparticles. Environ Sci Technol 2007;41(19):6841–6846. [PubMed: 17969704]
9. Shih YH, Tai YT. Reaction of decabrominated diphenyl ether by zerovalent iron nanoplarticles. Chemosphere 2010;78(10):1200–1206. [PubMed: 20117822]
10. Keum YS, Li QX. Reductive debromination of polybrominated diphenyl ethers by zerovalent iron. Environ Sci Technol 2005;39(7):2280–2286. [PubMed: 15871265]
11. Liu YQ, Majetich SA, Tilton RD, Sholl DS, Lowry GV. TCE dechlorination rates, pathways, and efficiency of nanoscale iron particles with different properties. Environ Sci Technol 2005;39(5): 1338–1345. [PubMed: 15787375]

12. Nurmi JT, Tratnyek PG, Sarathy V, Baer DR, Amonette JE, Pecher K, Wang CM, Linehan JC, Matson DW, Penn RL, et al. Characterization and properties of metallic iron nanoparticles: Spectroscopy, electrochemistry, and kinetics. Environ Sci Technol 2005;39(5):1221–1230. [PubMed: 15787360]
13. Schrick B, Blough JL, Jones AD, Mallouk TE. Hydrodechlorination of trichloroethylene to hydrocarbons using bimetallic nickel-iron nanoparticles. Chem Mater 2002;14(12):5140–5147.
14. Lowry GV, Johnson KM. Congener-specific dechlorination of dissolved PCBs by microscale and nanoscale zerovalent iron in a water/methanol solution. Environ Sci Technol 2004;38(19):5208–5216. [PubMed: 15506219]
15. Sun YP, Li XQ, Zhang WX, Wang HP. A method for the preparation of stable dispersion of zero-valent iron nanoparticles. Colloid Surface A 2007;308(1–3):60–66.
16. Zhu BW, Lim TT. Catalytic reduction of chlorobenzenes with Pd/Fe nanoparticles: Reactive sites, catalyst stability, particle aging, and regeneration. Environ Sci Technol 2007;41(21):7523–7529. [PubMed: 18044536]
17. Wang CB, Zhang WX. Synthesizing nanoscale iron particles for rapid and complete dechlorination of TCE and PCBs. Environ Sci Technol 1997;31(7):2154–2156.
18. Wang Q, Snyder S, Kim J, Choi H. Aqueous ethanol modified nanoscale zerovalent iron in bromate reduction: Synthesis, characterization, and reactivity. Environ Sci Technol 2009;43(9):3292–3299. [PubMed: 19534149]
19. Ponder SM, Darab JG, Mallouk TE. Remediation of Cr(VI) and Pb(II) aqueous solutions using supported, nanoscale zero-valent iron. Environ Sci Technol 2000;34(12):2564–2569.
20. Yak HK, Wenclawiak BW, Cheng IF, Doyle JG, Wai CM. Reductive dechlorination of polychlorinated biphenyls by zerovalent iron in subcritical water. Environ Sci Technol 1999;33(8):1307–1310.
21. Zhu BW, Lim TT, Feng J. Reductive dechlorination of 1,2,4-trichlorobenzene with palladized nanoscale Fe^0 particles supported on chitosan and silica. Chemosphere 2006;65(7):1137–1145. [PubMed: 16735054]
22. Kim YH, Shin WS, Ko SO. Reductive dechlorination of chlorinated biphenyls by palladized zero-valent metals. J Environ Sci Health A-Tox/Hazard Subst Environ Eng 2004;39(5):1177–1188.
23. Zeng X, Freeman PK, Vasil'ev YV, Voinov VG, Simonich SL, Barofsky DF. Theoretical calculation of thermodynamic properties of polybrominated diphenyl ethers. J Chem Eng Data 2005;50(5):1548–1556.
24. Rayne S, Ikonomou MG, Whale MD. Anaerobic microbial and photochemical degradation of 4,4 ′-dibromodiphenyl ether. Water Research 2003;37(3):551–560. [PubMed: 12688689]
25. Hakk H, Letcher RJ. Metabolism in the toxicokinetics and fate of brominated flame retardants - a review. Environ Int 2003;29(6):801–828. [PubMed: 12850098]
26. Eriksson J, Green N, Marsh G, Bergman A. Photochemical decomposition of 15 polybrominated diphenyl ether congeners in methanol/water. Environ Sci Technol 2004;38(11):3119–3125. [PubMed: 15224744]
27. Haga N, Takayanagi H. Mechanisms of the photochemical rearrangement of diphenyl ethers. J Org Chem 1996;61(2):735–745. [PubMed: 11666998]
28. Joo SH, Feitz AJ, Waite TD. Oxidative degradation of the carbothioate herbicide, molinate, using nanoscale zero-valent iron. Environ Sci Technol 2004;38(7):2242–2247. [PubMed: 15112830]
29. Buser HR, Rappe C. Formation of polychlorinated dibenzofurans (PCDFs) from the pyrolysis of individual PCB isomers. Chemosphere 1979;8(3):157–174.
30. Minkin VI, Mikhailov IE, Dushenko GA, Yudilevich JA, Minyaev RM, Zschunke A, Mugge K. 1,5-Sigmatropic Shifts of Bromine over a Cyclopentadiene Ring. J Phys Org Chem 1991;4(1):31–47.
31. Kamei I, Kogura R, Kondo R. Metabolism of 4,4′-dichlorobiphenyl by white-rot fungi Phanerochaete chrysosporium and Phanerochaete sp MZ142. App Micro Biotech 2006;72(3):566–575.
32. Liu J, Hu DF, Jiang G, Schnoor JL. In vivo biotransformation of 3,3,4,4-tetrachlorobiphenyl by whole plants-poplars and switchgrass. Environ Sci Technol 2009;43(19):7503–7509. [PubMed: 19848168]
33. Yak HK, Lang QY, Wai CM. Relative resistance of positional isomers of polychlorinated biphenyls toward reductive dechlorination by zerovalent iron in subcritical water. Environ Sci Technol 2000;34(13):2792–2798.

34. Fu QS, Barkovskii AL, Adriaens P. Reductive transformation of dioxins: An assessment of the contribution of dissolved organic matter to dechlorination reactions. Environ Sci Technol 1999;33 (21):3837–3842.
35. Scherer MM, Balko BA, Gallagher DA, Tratnyek PG. Correlation analysis of rate constants for dechlorination by zero-valent iron. Environ Sci Technol 1998;32(19):3026–3033.
36. Liu YQ, Choi H, Dionysiou D, Lowry GV. Trichloroethene hydrodechlorination in water by highly disordered monometallic nanoiron. Chem Mater 2005;17(21):5315–5322.
37. Sohn K, Kang SW, Ahn S, Woo M, Yang SK. Fe(0) nanoparticles for nitrate reduction: Stability, reactivity, and transformation. Environ Sci Technol 2006;40(17):5514–5519. [PubMed: 16999133]
38. Liu YQ, Lowry GV. Effect of particle age (Fe^0 content) and solution pH on nZVI reactivity: $^{H}2$ evolution and TCE dechlorination. Environ Sci Technol 2006;40(19):6085–6090. [PubMed: 17051804]
39. Hu JW, Eriksson L, Bergman A, Jakobsson E, Kolehmainen E, Knuutinen J, Suontamo R, Wei XH. Molecular orbital studies on brominated diphenyl ethers. Part II - reactivity and quantitative structure - activity (property) relationships. Chemosphere 2005;59(7):1043–1057. [PubMed: 15823338]
40. Zhao YY, Tao FM, Zeng EY. Theoretical study on the chemical properties of polybrominated diphenyl ethers. Chemosphere 2008;70(5):901–907. [PubMed: 17707458]
41. Karelson M, Lobanov VS, Katritzky AR. Quantum-chemical descriptors in QSAR/QSPR studies. Chem Rev 1996;96(3):1027–1043. [PubMed: 11848779]

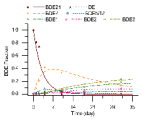

Figure 1.
Degradation of BDE 21 by nZVI and changes in byproducts formation. The y-axis represents the mole fraction of a certain BDE normalized by the initial moles of BDE 21. The lines indicate the modeling results according to the rate equations proposed in Equation S5 (derived from simplified pathways shown in Figure 2).

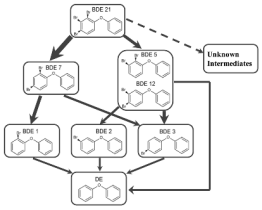

Figure 2.
Proposed debromination pathways of BDE 21 by nZVI. Broader arrows indicate major pathways. The formation of the unknown intermediates was considered in the proposed pathways but not confirmed (represented in dotted line).

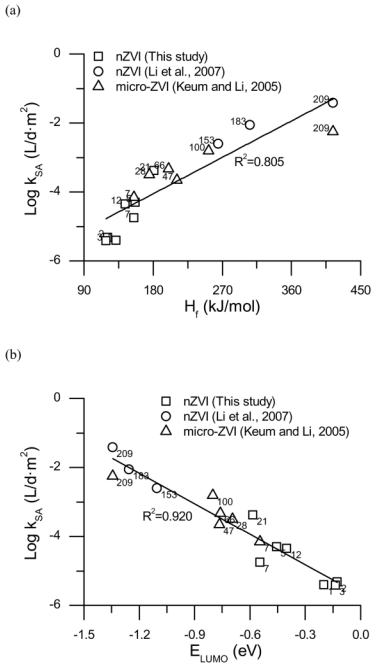

Figure 3.

Correlations between surface area normalized debromination rate constants and (a) heat of formation, H_f, and (b) energy for lowest unoccupied molecular orbital, E_{LUMO} (Values of H_f and E_{LUMO} of BDEs were obtained from Hu et al. (39)).

Table 1

Estimated debromination rate constants for mono-, di-, and tri-BDEs. The observed rate constants (k_{obs}) were normalized by the mass of nZVI (k_m) and by the surface area (k_{SA}) of nZVI in the system.

IUPAC No.	PBDE congener	k_{obs} [1/d]	k_m [L/d·g]	k_{SA} [L/d·m^2]	Reference
BDE 1	2-monoBDE	2.80 E-03	5.09 E-05	3.97 E-06	This study
BDE 2	3-monoBDE	3.40 E-03	6.18 E-05	4.82 E-06	
BDE 3	4-monoBDE	2.70 E-03	4.91 E-05	3.83 E-06	
BDE 5	2,3-diBDE	3.55 E-02	6.45 E-04	5.03 E-05	
BDE 7	2,4-diBDE	1.26 E-02	2.29 E-04	1.79 E-05	
BDE 12	3,4-diBDE	3.14 E-02	5.72 E-04	4.46 E-05	
BDE 21	2,3,4-triBDE	2.95 E-01	5.37 E-03	4.19 E-04	
BDE 153	2,2′,4,4′,5,5′-hexaBDE	4.32 E-01	3.14E-02	2.45E-03	(8)[a]
BDE 183	2,2′,3,4,4′,5′,6-heptaBDE	1.54	1.12E-01	8.71E-03	
BDE 209	DecaBDE	6.67	4.85E-01	3.78E-02	
BDE 7	2,4-diBDE	1.80 E-03	3.56E-06	6.93E-05	(10)[b]
BDE 28	2,4,4′-triBDE	7.90 E-03	1.59E-05	3.10E-04	
BDE 47	2,2′,4,4′-tetraBDE	5.60 E-03	1.12E-05	2.19E-04	
BDE 66	2,3′,4,4′-tetraBDE	1.20 E-02	2.40E-05	4.69E-04	
BDE 100	2,2′,4,4′,6-pentaBDE	3.98 E-02	7.96E-05	1.55E-03	
BDE 209	DecaBDE	1.41 E-01	2.83E-04	5.51E-03	

Note:

[a] nZVI mass = 0.014 g/ml, Avg. size = 60 nm;

[b] micro-ZVI mass = 0.5 g/ml, Avg. size = 15μm.